Engineered EGF-A peptides with improved affinity for proprotein convertase subtilisin/kexin type 9 (PCSK9)

Benjamin J. Tombling,[1] Carmen Lammi,[2] Nicole Lawrence,[1] Jianqiang Li,[2] Anna Arnoldi,[2] David J. Craik,[1] Conan K. Wang[1]*

[1] Institute for Molecular Bioscience, Australian Research Council Centre of Excellence for Innovations in Peptide and Protein Science, The University of Queensland, Brisbane, Qld, 4072, Australia.

[2] Dipartimento di Scienze Farmaceutiche, Università degli Studi di Milano, Via L. Mangiagalli 25, 20133 Milan, Italy

* Corresponding author: c.wang@imb.uq.edu.au

Abstract

The epidermal growth factor-like domain A (EGF-A) of the low-density lipoprotein (LDL) receptor is a promising lead for therapeutic inhibition of proprotein convertase subtilisin/kexin type 9 (PCSK9). However, the clinical potential of EGF-A is limited by its sub-optimal affinity for PCSK9. Here we use phage display to identify EGF-A analogues with extended bioactive segments that have improved affinity for PCSK9. The most potent analogue, TEX-S2_03, demonstrated ~130-fold improved affinity over the parent domain, and had a reduced calcium dependency for efficient PCSK9 binding. Thermodynamic binding analysis suggests the improved affinity of TEX-S2_03 is enthalpically driven, indicating favorable interactions are formed between the extended segment of TEX-S2_03 and the PCSK9 surface. The improved affinity of TEX-S2_03 resulted in increased activity in competition binding assays, and more efficient restoration of LDL receptor levels with clearance of extracellular LDL cholesterol in functional cell assays. These results confirm that TEX-S2_03 is a promising therapeutic lead for treating hypercholesterolemia. Many EGF-like domains are involved in disease-related protein–protein interactions; therefore, our strategy for engineering EGF-like domains has the potential to be broadly implemented in EGF-based drug design.

INTRODUCTION

Cardiovascular disease (CVD) remains one of the largest health burdens around the world.[1] A major risk factor of CVD is low-density lipoprotein (LDL) cholesterol (LDL-C), as elevated LDL-C levels in circulation can lead to chronic diseases such as atherosclerosis.[2] Statins are widely prescribed for lowering LDL-C to prevent CVD events; however, efficacy limitations of statins have stressed the importance of developing new therapies for treating CVD.[3, 4] Proprotein convertase subtilisin/kexin type 9 (PCSK9) is the major regulator of the LDL receptor (LDLR) which subsequently affects its ability to efficiently remove LDL-C from circulation,[5-7] and individuals with gain-of-function mutations of PCSK9 have significantly elevated LDL-C levels and increased risk of atherosclerosis.[8] This causal connection suggested that inhibition of PCSK9 will lower LDL-C levels. Subsequent genomic, functional, and clinical studies have validated PCSK9 as one of the most promising new therapeutic targets for cholesterol-lowering therapy.[9-11]

PCSK9 regulates LDLR levels by binding to the extracellular domain of LDLR at liver cell surfaces and prevents receptor recycling – an endocytic pathway fundamental to the efficient removal of LDL-C from the blood.[12, 13] The dominant binding site in the extracellular milieu occurs between the catalytic domain of PCSK9 and the first epidermal growth factor-like domain (EGF-A) of LDLR,[13, 14] which is a protein microdomain located in the EGF precursor homology region.

The binding interaction between PCSK9 and EGF-A constitutes a flat and featureless interface of ~500 Å^2 that has made small molecule intervention highly challenging to date.[15-17] Clinically approved monoclonal antibodies that bind to PCSK9 and prevent LDLR interaction

have shown good efficacy in lowering LDL-C and reducing the number of CVD events experienced by hypercholesterolemic patients.[18-21] However, their clinical use has been underwhelming, in part due to their high price which has raised concerns regarding their cost-effectiveness.[22, 23] These drawbacks have stimulated research into identifying alternative therapeutic modalities for inhibiting PCSK9.[24, 25]

Peptides have great potential as drugs,[26, 27] and some have gained attention as promising modulators of PCSK9. The ability of peptides to mimic complex protein structures engenders them with the ability to block protein–protein interactions (PPIs) with high specificity,[28] and their smaller size compared to antibodies allows them to be produced more cheaply. For these reasons, there has been wide interest in developing peptide-based PCSK9 inhibitors using multiple platforms, such as high-throughput combinatorial library screening,[29-32] computationally derived peptidomimetics,[33, 34] or peptide fragments from food-derived proteins.[35-37] However, peptide leads discovered to date are yet to be clinically available, partly due to poor pharmaceutical properties such as low affinity, solubility and stability. Therefore, the discovery of new leads and optimization of current leads is urgently needed.

A promising lead for the development of peptide-based PCSK9 inhibitors is the EGF-A domain of LDLR. Not only is this domain a natural lead for inhibitor design but it belongs to a structural family of disulfide-rich domains that have several properties that make them valuable scaffolds for molecular engineering and therapeutic development. First, their participation in PPIs means they are well-suited to binding to protein surfaces without prominent structural features that are typically challenging to target.[17, 38, 39] Second, they are characterized by a conserved disulfide-rich framework that engenders them with advantageous pharmaceutical properties

such as improved stability and increased structural rigidity.[40-42] Third, the segments between conserved cysteine residues of EGF-like domains show high levels of variability in terms of length and amino acid composition. For example, the length of segment 2, which sits between Cys^{I} and Cys^{II}, ranges from 0 to 14 amino acids, and the length of segment 3, which sits between Cys^{II} and Cys^{III}, ranges from 2 to 16 amino acids.[43] The sequence diversity of the segments suggests that EGF-like domains can tolerate modification by inserting foreign peptide motifs between conserved Cys residues. This concept has been extensively explored for other disulfide-rich peptide scaffolds such as cyclotides.[44] In short, EGF-like domains are highly abundant throughout nature, but their use as scaffolds for peptide drug design is surprisingly underexplored.

In a 2008 study, an excised EGF-A domain was shown to prevent PCSK9 binding to LDLR and restore cellular LDLR function.[45] Subsequent efforts have explored optimizing EGF-A to improve its affinity and activity; for example, PCSK9 binding residues of EGF-A were optimized using a combinatorial library screening approach which identified analogues with improved affinity for PCSK9.[46] However, the most potent compounds endured synthesis difficulties and as a result Fc-fusion constructs were required for activity determination. As an alternative strategy, we truncated the EGF-A domain by removing the C-terminal region (consisting of the third disulfide bond and last two segments), resulting in a smaller analogue (tEGF-A) that was easier to chemically synthesize.[47] However, the truncated analogue resulted in no improvement in affinity for PCSK9 over the full-length domain. Overall, the sub-optimal properties of these EGF-A analogues highlights the need to investigate alternative approaches to improve activity.

In this study we show that bioactive segments of the EGF-A analogue, tEGF-A, can be engineered to optimize its binding interface with PCSK9. We produced and screened phage display libraries with extended segments to expand the contact interface with PCSK9 resulting in the identification of tEGF-A analogues that have improved affinity for PCSK9 *in vitro* and increased efficacy in functional cell-based assays. These results provide new insights and guidance for designing EGF-A analogues that have the potential to be developed into new cholesterol-lowering therapeutics.

RESULTS

Designing extended tEGF-A scaffolds for high throughput screening

Analysis of the tEGF-A:PCSK9 crystal structure (PBD 4NE9) shows that segments 2 and 3 of tEGF-A are orientated close to the PCSK9 surface and residues from these segments are important for protein binding (see Figure 1).[16, 46, 48] Therefore, we hypothesized that these segments could be the subject of molecular engineering by extending their lengths to identify optimized segments capable of improved interaction with PCSK9. Two TEX (truncated EGF-A extension) phage libraries were constructed: TEX-S2 (where the length of segment 2 was increased from 6 to 14 residues, see Figure 2A) and TEX-S3 (where the length of segment 3 was increased from 3 to 11 residues, see Figure 2B).

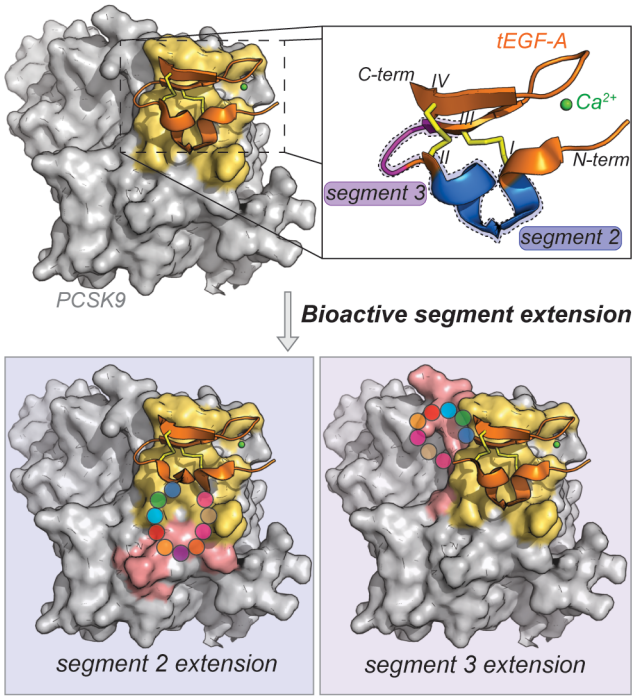

Figure 1. A bioactive segment extension approach for improving the affinity of truncated EGF-A (tEGF-A) by increasing and optimizing the binding interface with PCSK9. Residues from segments 2 (blue) and 3 (purple) of tEGF-A (orange) contact PCSK9 (PDB 4NE9) and these segments were re-engineered to increase binding affinity by extending their lengths. The

PCSK9 surface contacting tEGF-A is highlighted yellow, with the non-utilized surface accessible to binding highlighted pink.

The TEX libraries were separately subjected to three rounds of panning against human PCSK9. Since calcium is required for stabilizing the tEGF-A fold and facilitates efficient binding to PCSK9,[48] we chemically re-folded the TEX libraries in the presence of calcium prior to each panning round to improve the likelihood of forming the desired disulfide connectivity. Furthermore, calcium was included during panning to facilitate binding between the displayed peptides and PCSK9. To selectively identify PCSK9 inhibitory binders, the bound phage were eluted with varied concentrations of synthetic tEGF-A. MiSeq next-generation sequencing was used to analyze output phage from each round (Supplementary Tables S1 and S2). Interestingly, the output phage from the TEX-S2 library were enriched for sequences with an additional pair of Cys residues at positions 10 and 11 or 10 and 15 of the extended segment (Figure 2A). The TEX-S3 library showed enrichment of a –HXHXH– motif in the randomized segment (Figure 2B). The most enriched sequences from each library that contained unique segment motifs (three sequences from TEX-S2 and two sequences from TEX-S3, see Figure 2C) were selected for chemical synthesis and binding validation.

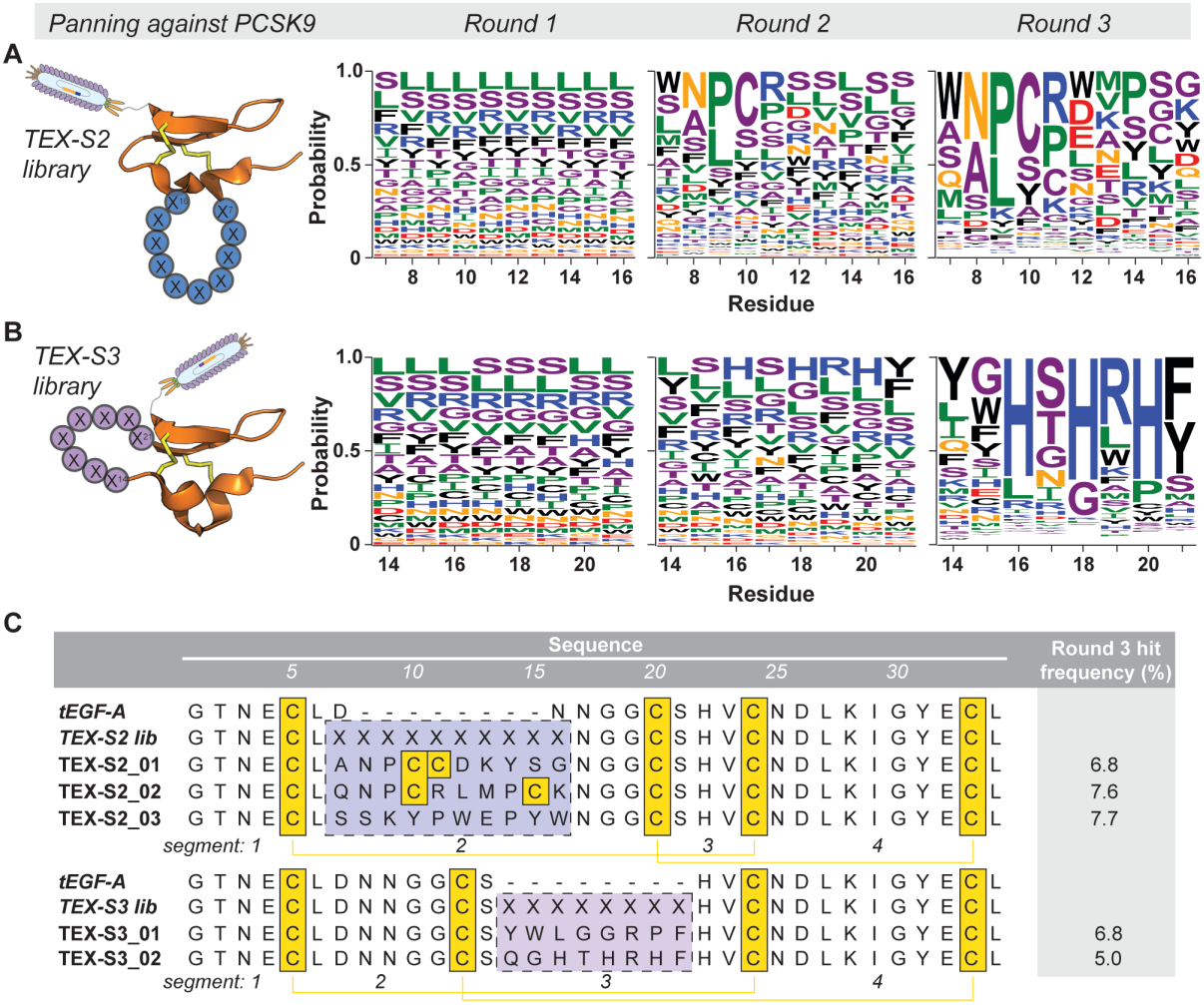

Figure 2. Screening tEGF-A extension (TEX) libraries against PCSK9. (A) TEX-S2 and (B) TEX-S3 libraries with 8 randomized residues inserted into segment 2 or 3 of tEGF-A, respectively. The MiSeq next generation sequencing data for the randomized segment motif is summarized based on the frequency of amino acids occurrence using sequence logos. (C) The most enriched peptide sequences from each phage displayed library after three rounds of panning are shown, with the final output library frequency shown in the right-hand column. The randomized extension motifs are surrounded by a box. X indicates a randomized residue. All Cys are highlighted in yellow with expected disulfide connectivity, based on the parent tEGF-A scaffold, indicated with yellow lines. The additional Cys residues of TEX-S2_01 and TEX-S2_02 were presumed to form an intra-segment disulfide bond.

Structural effects of segment extension on EGF-fold

Phage derived peptides TEX-S2_01–03 and TEX-S3_01–02 were chemically synthesized using standard Fmoc SPPS. To form the desired disulfide connectivity, the peptides that contained four Cys residues were oxidized using orthogonal disulfide bond formation (see Supplementary Table S3). Due to the additional Cys residues in the extended segments of TEX-S2_01 and TEX-S2_02, disulfide connectivity was not enforced during synthesis and oxidation of these peptides was performed in a one-step redox environment that contained calcium to help form the desired disulfide connectivity (Supplementary Figure S1).

To analyze whether the TEX peptides retained the structural topology of the EGF-fold, 1D ^{1}H NMR spectra were recorded and compared to tEGF-A. Our previous studies showed that low temperatures and the presence of calcium are important for stabilizing the tEGF-A conformation;[47, 48] therefore, spectra were recorded at 283 K with 5 mM $CaCl_2$. As shown in Figure 3A, all TEX peptides had poorly defined structures compared to tEGF-A, indicated by the broad peaks and narrow spectral dispersion in the amide signal region. Broad signals often reflect the presence of slow/intermediate exchange between multiple conformations, which suggests the TEX peptides are flexible in solution. Interestingly, the additional disulfide bond in TEX-S2_01 and TEX-S2_02 appeared to have little effect on stabilizing the structure. The TEX-S3 peptides had slightly sharper peaks; however, they still suffered from poor dispersion and secondary structure analysis was not viable. The upfield Hα chemical shifts present in the tEGF-A spectrum that represent the presence of a ß-sheet motif were not present for all the TEX peptides, further indicating TEX peptides are more flexible than their parent peptide.

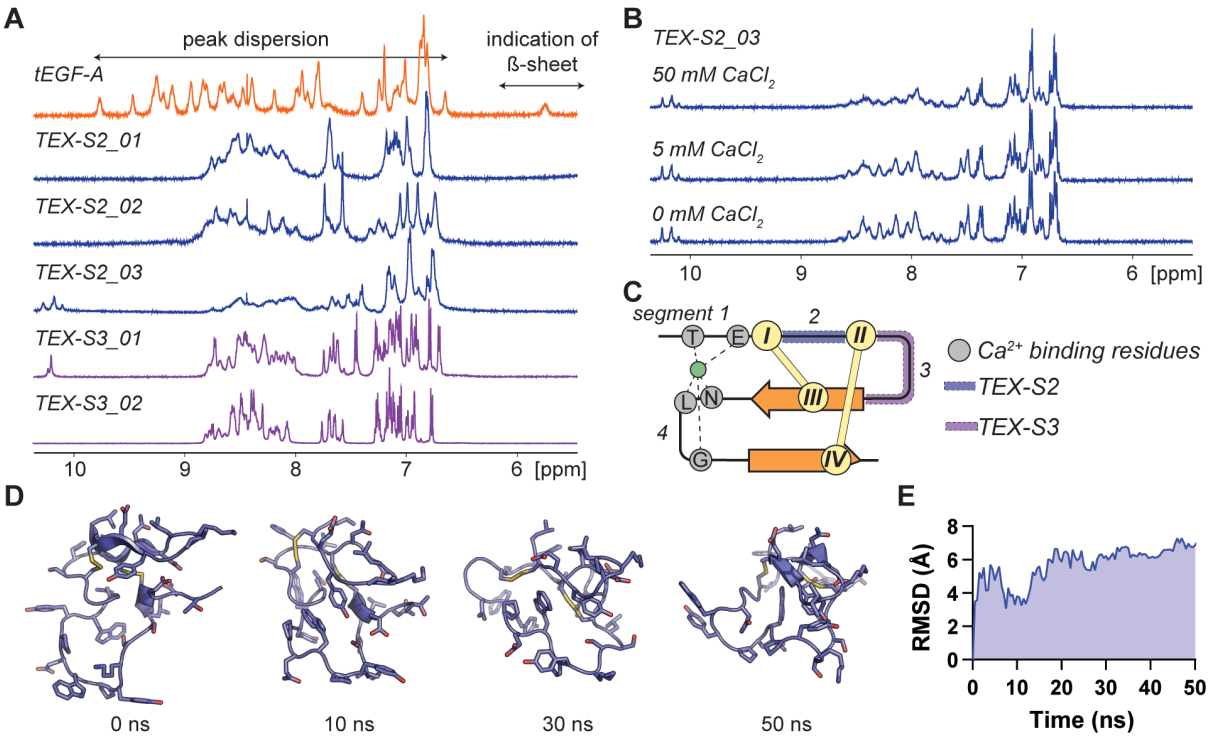

Figure 3. Structural analysis of TEX peptides. (A) 1D ^{1}H NMR spectra for tEGF-A (orange) and TEX-S2 (blue) and TEX-S3 (purple) peptides. An upfield Hα chemical shift that represents the presence of a ß-sheet is identified on the tEGF-A spectrum. All spectra were recorded at 283 K with 5 mM $CaCl_2$. (B) Effects of calcium on the structure of TEX-S2_03 by analyzing differences in the 1D spectra. Spectra were recorded at 298 K as temperature did not affect spectra quality (see Supplementary Figure S2). (C) Illustration of the calcium binding residues on tEGF-A (grey), showing that they are not part of the engineered segments. (D) Cartoon representations of TEX-S2_03 at 0, 10, 30 and 50 ns time points taken from molecular dynamic simulations. (E) Root-mean-square deviation (RMSD) (Å) for backbone atoms of TEX-S2_03 over the course of the simulations compared to the initial in-silico structure.

We selected TEX-S2_03 for structure characterization in diverse chemical and thermal conditions since this compound was the most active (see binding data below). Because calcium is important for stabilizing tEGF-A, we compared the 1D ^{1}H NMR spectra of TEX-S2_03 in

the presence of 0, 5 and 50 mM $CaCl_2$. However, no major differences were observed (Figure 3B), even though TEX-S2_03 inherits the five residues of tEGF-A known to be involved in a bipyramidal coordination to calcium (Thr and Glu in segment 1; and Asn, Leu, Gly in segment 4),[48] as shown in Figure 3C. It is possible the increased structural flexibility counteracts the stabilizing effects of calcium binding. Additional experiments that examined the effects of temperature, pH and hydrophobicity had little effect on spectral quality (Supplementary Figure S2). In general, the spectra of TEX-S2_03 were characterized by broad peaks, which are due to conformational exchange in the slow to intermediate timescale of NMR, suggesting TEX-S2_03 is flexible in a wide range of solution conditions. In agreement with the NMR analysis, TEX-S2_03 exchanged between multiple conformations during molecular dynamic (MD) simulations (Figure 3D and 3E) and provided further evidence that the TEX peptides can be flexible despite having an EGF-like fold.

High proteolytic stability is often a hallmark of natively folded disulfide-rich peptides. Therefore, TEX-S2_03 and TEX-S3_01 were monitored for their stability in human serum, and compared to tEGF-A, to see if the increased flexibility leads to an increased susceptibility to proteolytic attack. Neither TEX-S2_03 or TEX-S3_01 were markedly degraded after 24 h incubation with human serum, showing similar stability to tEGF-A (Supplementary Figure S3). The only notable observation was the emergence of a by-product with a ΔMW of +1 during TEX-S2_03 incubation with serum over 24 h, most likely indicating deamidation of an Asn sidechain. Together, these results suggest that although segment extension of tEGF-A distorted the EGF-fold and reduced structural rigidity, it did not affect proteolytic stability. Although the TEX peptides were more flexible than their parent peptide, we hypothesized structural rigidification might occur upon binding to PCSK9 much like how many peptide ligands change

conformation upon contact with their cognate receptor. Therefore, we proceeded to test the activity of the TEX peptides.

TEX-S2 peptides have improved affinity for PCSK9

The affinity of the TEX peptides for PCSK9 were determined using surface plasmon resonance (SPR) and competitive enzyme-linked immunosorbent assay (ELISA) binding experiments. SPR sensorgrams showing the binding (association, dissociation) of TEX peptides to PCSK9 in the presence of 5 mM $CaCl_2$ are presented in Figure 4A. Interestingly, all TEX-S2 peptides had improved affinities for PCSK9 compared to tEGF-A. Remarkably, the most potent peptide, TEX-S2_03, had an equilibrium dissociation constant (K_D) of 15 nM, which is ~130-fold lower than tEGF-A (K_D of 1,965 nM) (Figure 4B). The improved affinity of TEX-S2_03 was due to a (favorable) ~500-fold slower dissociation rate (k_{off}) compared to tEGF-A, which offsets the ~5-fold slower association rate (k_{on}) (see Table 1). In comparison, the improved affinities of TEX-S2_01 (K_D of 511 nM) and TEX-S2_02 (K_D of 280 nM) were solely due to faster k_{on}. The results for the TEX-S2 peptides were markedly more promising than those for the TEX-S3 peptides (TEX-S3_01 had a K_D of 3,383 nM and TEX-S3_02 showed no affinity for PCSK9 up to 54 μM).

Table 1. Kinetic parameters of TEX peptides binding to PCSK9 determined by SPR [a]

Peptide	k_{on} (x 10^4 M^{-1} s^{-1})	k_{off} (x 10^{-3} s^{-1})	K_D (μM)
With 5 mM $CaCl_2$			
tEGF-A	8.165 ± 2.7	148 ± 20	2.0 ± 0.7
TEX-S2_01	34.4 ± 2.3	176 ± 5	0.51 ± 0.02
TEX-S2_02	71.2 ± 2.2	188 ± 6	0.28 ± 0.08
TEX-S2_03	1.9 ± 0.1	0.3 ± 0.07	0.015 ± 0.003
TEX-S3_01	3.9 ± 1.4	111 ± 34	3.4 ± 1.0
TEX-S3_02	No binding up to 54 μM		
Without $CaCl_2$			
tEGF-A	No binding up to 54 μM		
TEX-S2_01	Not determined		

TEX-S2_02	1.5 ± 0.3	204 ± 39	13.6 ± 0.2
TEX-S2_03	0.28 ± 0.08	22 ± 0.07	8.3 ± 2.3
TEX-S3_01	No binding up to 54 μM		
TEX-S3_02	No binding up to 54 μM		

[a] k_{on} is the association rate constant, k_{off} is the dissociation rate constant, K_D is the equilibrium dissociation constant (used to compare binding affinity). Values were determined from single cycle SPR sensorgrams (see Figure 4A) using BIAevaluation software and are the average ± s.d. from at least two independent experiments.

The ability of the TEX peptides to bind to PCSK9 in a calcium-free environment was also assessed (Figure 4C), as calcium-dependent binding is a hallmark property of the parent peptide. In agreement with our previous studies,[47, 48] removal of calcium resulted in tEGF-A showing no affinity for PCSK9. In a similar fashion, both TEX-S2_02 and TEX-S2_03 had ~50-fold and ~500-fold lower affinities in the absence of calcium, though binding was not completely abolished. Both TEX-S2_02 and TEX-S2_03 had slower k_{on} in the calcium-free environment (see Table 1), suggesting that calcium plays a role in orientating these peptides for efficient interaction with PCSK9.

Selected TEX peptides were investigated for their ability to modulate the tEGF-A:PCSK9 interaction using a competition ELISA.[32] In agreement with the improved affinity determined during SPR, ~3-fold and ~10-fold lower concentrations of TEX-S2_02 and TEX-S2_03, respectively, were required to inhibit the binding of 50% of HA-tagged tEGF-A to PCSK9 (IC_{50}) compared to tEGF-A (TEX-S2_02 IC_{50} [95% confidence interval] of 2.1 [1.2, 21.3] μM, TEX-S2_03 IC_{50} of 0.6 [0.4, 1.0] μM, tEGF-A IC_{50} of 6.9 [5.4, 9.1] μM; Figure 4D). TEX-S3_01 (IC_{50} of 11.7 [8.7, 17.7] μM) showed reduced inhibitory activity compared to tEGF-A, whereas TEX-S3_02 showed no ability to block the tEGF-A:PCSK9 interaction. The

competition ELISA data suggested extension of segment 2 resulted in more potent peptides than extension of segment 3, with TEX-S2_03 being the most potent.

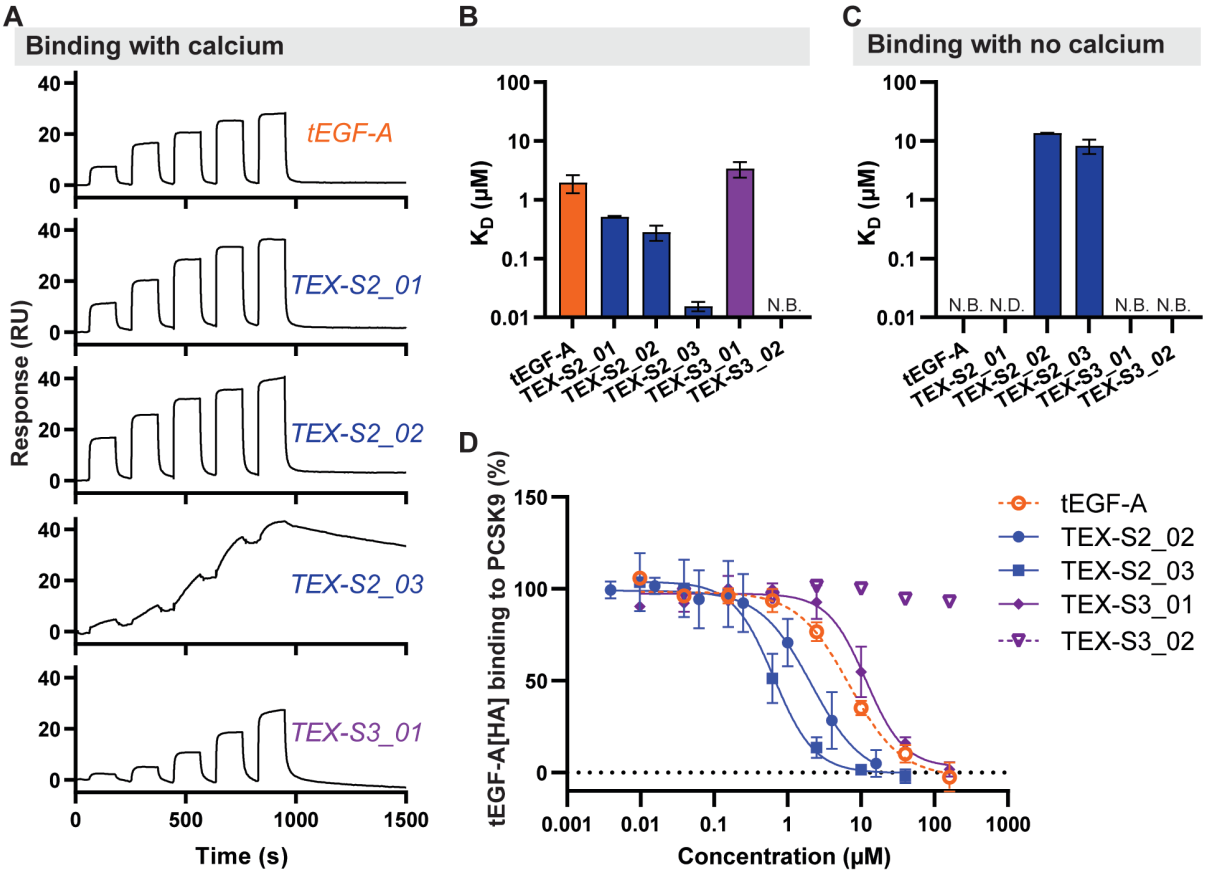

Figure 4. *In vitro* binding of TEX peptides to PCSK9. (A) Single cycle SPR sensorgrams showing peptide binding to immobilized PCSK9 in a calcium-present environment. All peptides were screened at 0.2, 0.7, 2, 6, and 18 μM, except TEX-S2_03 which was screened at 0.02, 0.07, 0.2, 0.7, and 2 μM. (B) Equilibrium dissociation constants, $K_D = k_{off}$ (dissociation constant)/k_{on} (association constant), for binding in a calcium-present environment. (C) K_D in a calcium-free environment. N.B. = no binding up to 54 μM; N.D. = not determined. (D) Dose response curves showing inhibition of PCSK9 binding to HA-tagged tEGF-A, tEGF-A[HA]. Data shown in panels B and C represent the average ± s.d. from at least two independent experiments. Data shown in panel D is the average ± s.d. from three independent experiments.

To characterize the molecular mechanism of increased TEX-S2_03 binding, we compared the thermodynamic binding parameters of tEGF-A and TEX-S2_03 for complex formation with PCSK9 using isothermal calorimetry (ITC) (Figure 5). TEX-S2_03 showed a more favorable enthalpic change (more negative ΔH), whereas the entropy contribution (more positive –TΔS) was more unfavored, compared to tEGF-A, suggesting that the improved affinity of TEX-S2_03 is enthalpically driven. These differences in thermodynamic parameters suggests that TEX-S2_03 forms more favorable non-covalent intermolecular interactions with PCSK9, as compared to tEGF-A, indicating an increased number of binding contacts.[49] In comparison, TEX-S2_01 showed similar thermodynamic binding parameters to tEGF-A (Supplementary, Figure S4). Together, the ITC data suggests that the extended segment of TEX-S2_03 is specifically accountable for the improved enthalpic contribution that drives the more energetically favored complex formation with PCSK9. Collectively, the *in vitro* binding assays indicated that TEX-S2_03 was the most promising peptide identified from the TEX libraries and showed dramatically improved site-specific binding affinity for PCSK9.

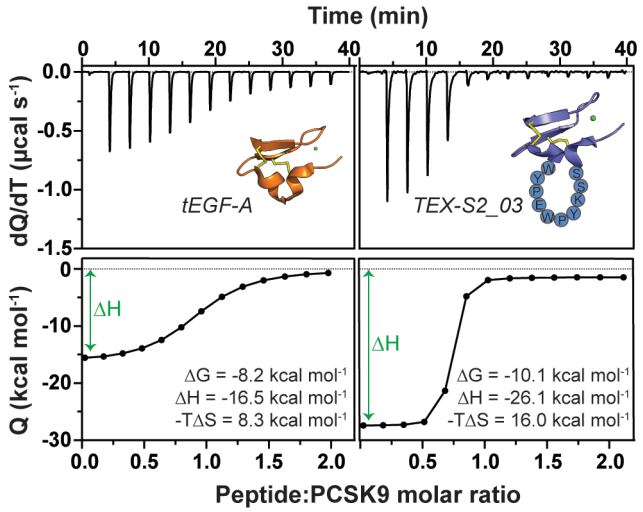

Figure 5. Thermodynamic binding analysis of tEGF-A and TEX_S2_03 binding to PCSK9. Binding isotherms show the differential power required to maintain system temperature (dQ/dT) and the integrated heat change per injection (Q). Contributions to the Gibbs free

energy change (ΔG) for the peptide:PCSK9 complex formation by the thermodynamic binding parameters enthalpy (ΔH) and entropy (–TΔS) are labeled on their respective graphs.

TEX peptides restore LDLR function

The peptide with the highest binding affinity for PCSK9, TEX-S2_03 (from the segment 2 extension library) was compared to tEGF-A for its ability to modulate the levels of LDLR localized on HepG2 (cultured liver cell) surfaces (Figure 6A). The most potent peptide from the segment 3 extension library, TEX-S3_01, was also tested for comparison. LDLR levels decreased in the presence of PCSK9 alone by 47.2 ± 1.5% compared to untreated control cells, and all tested peptides significantly increased LDLR levels when co-incubated with PCSK9. Specifically, tEGF-A and TEX-S3_01 showed moderate micromolar activity, with incomplete LDLR restoration (72.8 ± 3.1% and 73.7 ± 5.6%, respectively) at 5 µM, and full LDLR restoration (91.5 ± 11.5% and 96.5 ± 11.5%, respectively) at 50 µM. By comparison, 5 µM of TEX-S2_03 was sufficient to completely restore surface LDLR levels (95.1 ± 1.9%), providing evidence of its increased potency and efficacy for inhibiting PCSK9 and restoring LDLR (Figure 6B).

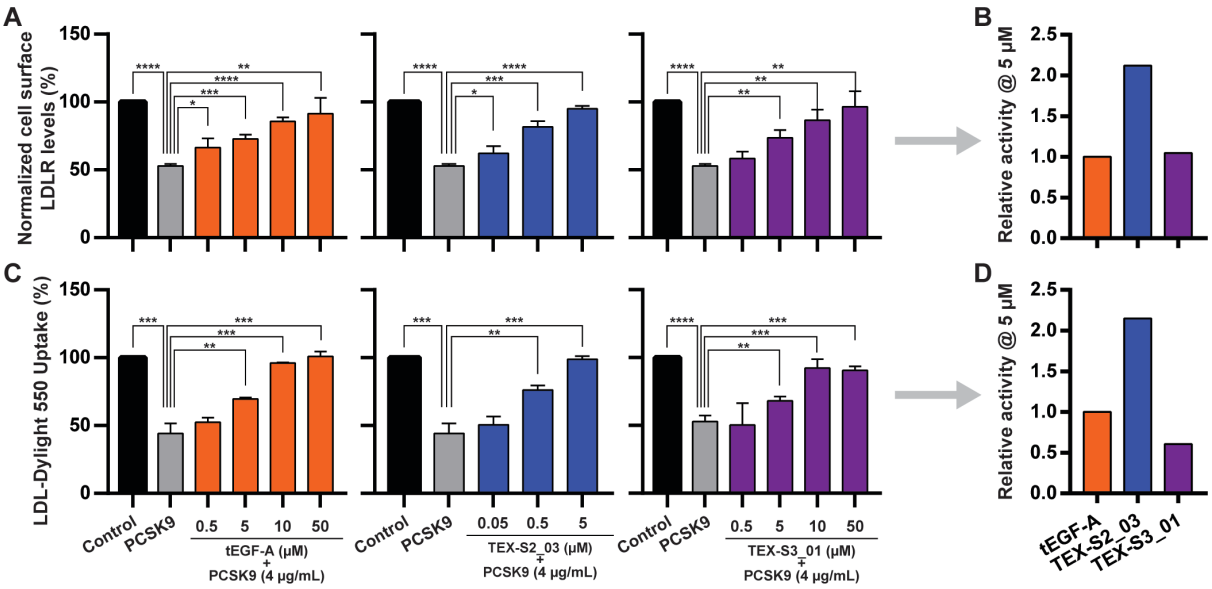

Figure 6. Restoration of LDLR function by TEX peptides compared to tEGF-A. tEGF-A (orange) data, TEX-S2_03 (blue) data, and TEX-S3_01 (purple) data are shown in the left, middle and right panels, respectively. (A) tEGF-A, TEX-S2_03, and TEX-S3_01 induce an increase of LDLR protein on HepG2 cell surfaces in the presence of PCSK9. (B) The relative increase in LDLR cell surface levels observed after treatment with 5 μM of tEGF-A, TEX-S2_03, or TEX-S3_01. (C) The decreased ability to uptake LDL by HepG2 cells induced by PCSK9 is prevented by increasing concentrations of tEGF-A, TEX-S2_03, and TEX-S3_01. (D) The relative increase in LDLR ability to internalize LDL observed after treatment with 5 μM of tEGF-A, TEX-S2_03, or TEX-S3_01. Control represents cells without any treatment. Results represent the average ± s.d. of three independent experiments, each performed in triplicate. Student t-test statistical analysis was performed; * $p < 0.05$, ** $p < 0.01$, *** $p < 0.001$, **** $p < 0.0001$.

The functional activity of the peptides was further assessed by monitoring their ability to modulate the capacity of HepG2 cells to uptake extracellular LDL in the presence of PCSK9 (Figure 6C). HepG2 cells incubated with PCSK9 showed a 55.8 ± 7.4% reduction in the uptake of fluorescent LDL compared to untreated cells, indicating reduced LDLR function. Treatment with 5 μM tEGF-A and TEX-S3_01 partly restored LDLR function, increasing LDL uptake to 69.6 ± 1.0% and 68.2 ± 3.1%, respectively. At the same peptide concentration, TEX-S2_03 completely restored LDL uptake (98.9 ± 2.3%; Figure 6D) and achieved 76.2 ± 3.5% of LDL uptake at the 10-fold lower concentration of 500 nM. Both TEX peptides were nontoxic to HepG2 cells at concentrations up to 50 μM (Supplementary Figure S5). Therefore, we conclude that the cell-based activity of TEX peptides is mediated by their ability to directly inhibit PCSK9. Furthermore, these functional assays confirm that the improved affinity of TEX-S2_03 for PCSK9 translates to improved biological activity and restoration of LDLR function.

DISCUSSION AND CONCLUSION

In this study, we re-engineered a truncated analogue of the EGF-A domain of LDLR to improve its ability to bind and inhibit PCSK9, promoting the uptake of LDL-C. By extending segments of tEGF-A involved in PCSK9 interaction, we designed phage-displayed peptide libraries to select for peptides with additional binding contacts and an extended interface with PCSK9. The most enriched sequences from two phage libraries were chemically synthesized and three out of the five selected peptides showed improved affinity for PCSK9. The most promising lead identified in this study, TEX-S2_03, has ~130-fold improved affinity for PCSK9 compared to parent tEGF-A, which led to increased ability to restore LDLR function in human liver cell-based assays.

The improved affinity of TEX-S2_03 for PCSK9, compared to the other TEX peptides and tEGF-A, can be directly attributed to the enriched residues incorporated into the extended segment. As evidenced by SPR (increased binding affinity, reduced k_{off}) and ITC (favorable enthalpic change), the stronger TEX-S2_03:PCSK9 interaction indicates segment 2 of TEX-S2_03 participates in additional binding events with PCSK9 that results in the overall formation of a larger binding interface. The extended segment of TEX-S2_03 is rich in aromatic residues (aa 7–16; SSKYPWEPYW); therefore, the more favorable enthalpic change observed for the complex formation may be driven by hydrophobic associations with the PCSK9 surface.

Competition binding assays confirmed that TEX-S2_03 bound to the native binding site occupied by tEGF-A and had improved antagonistic activity. Even though TEX-S2_03 binds to the same site as tEGF-A, our structural and activity data suggests a more elaborate binding mechanism is occurring. The flexible nature of TEX-S2_03 indicates that it affects the pre-

orientation of the functional residues for efficient binding to PCSK9. Therefore, it is likely that the engagement of TEX-S2_03 to PCSK9 is different to that of tEGF-A and requires local structural reorganization. This is evidenced by the TEX-S2_03:PCSK9 complex formation encountering a large entropic penalty, which might be due to structural restriction of TEX-S2_03 upon binding to PCSK9 and the slower k_{on} observed in SPR. This phenomenon is less evident for tEGF-A as it adopts similar conformations when bound and unbound to PCSK9.[47] We propose the new interactions between TEX-S2_03 and PCSK9 help TEX-S2_03 overcome its entropic penalty. These new binding interactions could expand into a binding pocket on PCSK9 outside of the tEGF-A:PCSK9 interface because TEX-S2_03 retains some affinity for PCSK9 in a calcium-free environment. An example of a potential site for expansion is the cryptic site occupied by the flexible P' helix of the PCSK9 catalytic domain which has recently been successfully targeted.[30, 50] To summarize, the binding mechanism might involve multiple binding stages; for example, first the extended segment of TEX-S2_03 contacts PCSK9, then the TEX peptide coordinates calcium on the PCSK9 surface, thereby promoting reorganization of the peptide into a more active conformation with higher affinity for PCSK9 (Figure 7). Despite not having validation of the mechanism of action, our results show we have successfully engineered a truncated EGF peptide from LDLR into a more promising therapeutic lead for lowering cholesterol.

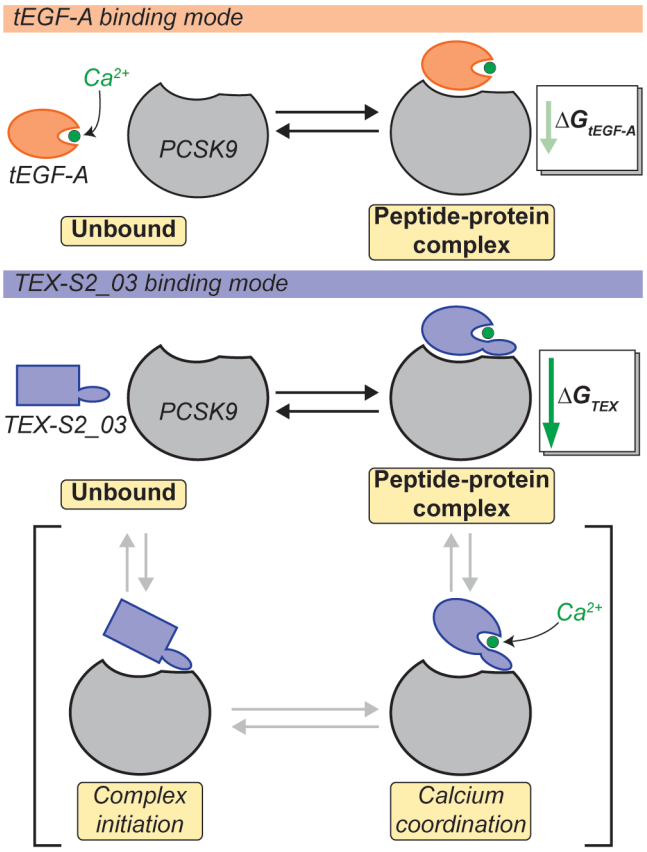

Figure 7

Cartoon illustration of proposed TEX-S2_03 binding mechanism to PCSK9 compared to tEGF-A. In solution, tEGF-A binds calcium which reorganizes the peptide tertiary structure to occupy the binding site located on PCSK9. On the contrary, the flexible structure of TEX-S2_03 in the unbound state means the peptide is not initially structured to efficiently interact with PCSK9. Instead, it appears that TEX-S2_03 weakly contacts PCSK9 (complex initiation) before calcium coordination takes place. This enables structural reorganization of TEX-S2_03 to form the most active conformation which forms an increased number of binding interactions with PCSK9 compared to tEGF-A. Despite the alternative binding mechanism, TEX-S2_03:PCSK9 complex formation is energetically more favored than tEGF-A, as evidenced by the more negative ΔG observed during ITC binding experiments (see Figure 5).

The successful application of the bioactive segment extension approach demonstrated here highlights its potential to be adopted as a tool for enhancing the affinity of other EGF-like domains involved in PPIs, including a large proportion that have calcium-independent mechanisms of action.[43] An example is the excised fifth EGF domain of thrombomodulin. It displays pro-angiogenetic and cytoprotective activities by inhibiting the thrombomodulin:thrombin interaction.[51, 52] Segment 6 of EGF5 is the major segment responsible for binding to thrombin and therefore, could be engineered using the bioactive segment extension approach for binding interface optimization. Overall, our bioactive segment extension strategy is a valuable addition to the growing repertoire of peptide affinity optimization approaches that increase the binding interface and lead to improved biological activity.

EXPERIMENTAL SECTION

Peptide phage library construction and screening

TEX phage libraries were designed based on the tEGF-A scaffold and produced as previously described.[32] TEX-S2 library contained a randomized 8-mer peptide motif inserted between Leu319 and Asn321 of segment 2 of tEGF-A and TEX-S3 library contained a randomized 8-mer peptide motif inserted between Ser326 and His327 of segment 3 of tEGF-A (amino acid numbering is based on LDLR; UniProt P01130). TEX-S2 and TEX-S3 were sub-cloned into pComb3X and transformed into XL-1 Blue cells using electroporation. The diversity of TEX-S2 and TEX-S3 libraries were 7.3×10^8 and 4.4×10^8, respectively. Both DNA libraries were propagated with VCSM13 helper phage. The propagated phage libraries were chemically re-folded by reducing with 1 mM TCEP for 1 h at room temperature (RT), precipitated with 20% PEG8000 2.5 M NaCl, and resuspended in 30 mL oxidation buffer (0.1 M Tris pH 8.2, 0.2 M NaCl, 10 mM $CaCl_2$, 2 mM reduced glutathione, 0.2 mM oxidized glutathione) for 24 h at RT. Both libraries were individually subjected to three panning rounds against biotinylated human PCSK9 immobilized onto Dynabeads (MyOne Streptavidin T1, Invitrogen). PCSK9 was used at 100, 50, and 20 nmol for rounds one, two and three, respectively. A competitive elution strategy was performed by incubating the bound phage with tEGF-A (200 µL for 10 min, tEGF-A concentrations used for competitive elution are shown in Supplementary Tables S1 and S2). Pooled output phage from each round were subjected to amplicon sequencing targeting the variable TEX coding regions using the Illumina MiSeq platform at the Australian Genome Research Facility. Probability of residues occupying each position of the variable region was visualized with WebLogo.[53]

Peptide synthesis, oxidation, and purification

Peptides were synthesized using standard Fmoc solid-phase peptide synthesis on rink amide resin at 0.125 mmol scale on a Symphony Multiplex Synthesizer. tEGF-A, TEX-S2_03, TEX-S3_01 and TEX-S3_02 were synthesized with Cys^{I} and Cys^{III} side chains protected with acetamidomethyl (Acm) to allow stepwise disulfide bond formation. The assembled peptides were deprotected and cleaved from the resin using trifluoroacetic acid (TFA):triisopropylsilane:H_2O (95:2.5:2.5 v/v) for 3 h at RT before precipitating with cold diethyl ether. Peptides were purified by reverse-phase high-performance liquid chromatography (RP-HPLC) on a Shimadzu Prominence system using a 0.5–1% min^{-1} linear gradient from 0.05% TFA in water (v/v) to 0.05% TFA in 90% acetonitrile (v/v).

TEX-S2_01 and TEX-S2_02 were oxidized using a one-step strategy at 0.2 mg mL^{-1} in oxidation buffer outlined above for 24 h. For the remaining peptides, the first disulfide bond was formed using oxidation buffer (0.2 mg mL^{-1}) for 24 h before acidifying and forming the second disulfide bond using I_2 for 30 min at RT. All oxidized peptides were purified by RP-HPLC. Peptide purities (> 95%) were determined by analytical RP-HPLC and peptide masses were confirmed by electrospray ionization mass spectrometry (ESI-MS) (Supplementary Figure S6). A list of peptides synthesized for this study is shown in Supplementary Table S3.

PCSK9 expression, purification and biotinylation

Full length human PCSK9 was expressed by The University of Queensland Protein Expression Facility (PEF), and subsequently purified and post-translationally biotinylated as previously described.[32] Briefly, crude secreted protein was purified by nickel affinity chromatography and size exclusion chromatography using a Sephacryl S-200 column (GE Healthcare). PCSK9 was

site-specifically biotinylated at an AviTag conjugated to the C-terminus using standard protocol with BirA enzyme. Briefly, PCSK9 (5 μM) and BirA (1:100, enzyme to protein molar ratio) were mixed before Biotin (60 eq.) and ATP (1000 eq.) were added and the reaction was left for 12 h at room temperature. Biotinylated PCSK9 was purified by SEC as described above.

NMR spectroscopy

The preliminary 1D ^{1}H NMR experiments were recorded at 283 K on a Bruker Advance 500 or 600 MHz spectrometer. Peptides were dissolved to 0.5–1 mM in 550 μL H_2O:D_2O (9:1 v/v) containing 5 mM $CaCl_2$. Further experiments were performed on TEX-S2_03 where the temperature was monitored at 283, 298, and 308 K, pH was adjusted using TFA and NaOH, and $CaCl_2$ was tested at 0, 5, and 50 mM. NMR spectra were also recorded for TEX-S2_03 in H_2O:acetonitrile-d_3 (7:3 v/v). All spectra were referenced to 4,4-dimethyl-4-silapentane-1-sulfonic acid (DSS) at 0 ppm.

Molecular dynamic simulations

An in-silico model of TEX-S2_03 was generated based on the structure of tEGF-A bound to PCSK9 (PDB 4NE9) using MODELLER.[54] Simulations were carried out as previously described.[48] tEGF-A or TEX-S2_03 were solvated in a 50 $Å^3$ water box. An equilibrium with stepwise relaxation was performed at the start of each simulation. All non-hydrogen atoms were restrained with a force constant of 2 kcal mol^{-1} $Å^{-2}$ and 5,000 system minimization steps were conducted using ACEMD v3.2.3[55] and CHARMM36 force field parameters. System temperature of 315 K was maintained using a Langevin thermostat with a friction coefficient of 0.1 ps^{-1}, and system pressure of 1 bar was maintained using an isotropic barostat. Long range-electrostatic interactions were computed using the particle mesh Ewald algorithm at

every timestep (4 fs), and smoothing was applied between 7.5 and 9 Å. Simulation production runs of 50 ns were conducted, and coordinates were saved every 500 ps. The root-mean-square deviation (RMSD) of all non-hydrogen backbone atoms were analyzed using Visual Molecular Dynamics (VMD).[56]

Human serum stability assay

Human serum (Sigma) was centrifuged at 14,000 *g* for 10 min to remove the lipid component. Serum supernatant was incubated at 37 °C for 15 min before incubating with peptides. Stock solutions of peptides (500 µM in H_2O) were added to prepared serum (1:9, v/v) to make a final volume of 40 µL and incubated at 37 °C for 0, 1, 2, 4, 8, and 24 h. tEGF-A was recovered from samples by adding 40 µL of 6 M urea (10 min, 4 °C) then 40 µL 20% trichloroacetic acid (w/v) (10 min, 4 °C) to precipitate serum proteins. TEX-S2_03 and TEX-S3_01 samples were recovered by adding 80 µL acetonitrile:TFA (97:3 v/v) (10 min, 4 °C). Samples were centrifuged at 14,000 *g* for 10 min and 100 µL of supernatant was analyzed using RP-HPLC using a 1% linear gradient from 0.05% TFA in 10% acetonitrile (v/v) to 0.05% TFA in 50% acetonitrile (v/v). Peptides were tested in triplicate.

SPR binding analysis

All SPR experiments were performed using a Biacore T200 instrument at 25 °C. Biotinylated human PCSK9 was captured (~1500 RU) on a streptavidin sensor chip (GE healthcare). Five serial three-fold dilutions of peptide were flowed over the PCSK9 surface using a single cycle kinetics model. Peptides were initially tested in a 20 mM HEPES pH 7.4, 100 mM NaCl, 5 mM $CaCl_2$, 0.05% Tween-20 (v/v) running buffer. All peptides were analyzed from low to high concentration and each concentration was injected for 120 s at a flow rate of 30 µL min^{-1}. All

peptides were tested at a maximum concentration of 18 μM, except TEX-S2_03 and TEX-S3_02 which were tested from 2 μM and 54 μM, respectively. For calcium-free binding experiments, the running buffer was prepared without calcium and all peptides were tested up to 54 μM. For all experiments, a streptavidin-bound reference channel was subtracted from the channel with captured PCSK9. Data were analyzed using GE BIAevaluation software using a 1:1 binding model. The K_D values, calculated from the determined k_{on} and k_{off} values using the equation $K_D = k_{off} / k_{on}$, were the average ± s.d. of at least two independent experiments.

ELISA competition assay

Competition binding experiments were performed as previously described.[32] Briefly, PCSK9 (3 μg mL^{-1}) was immobilized to Neutravidin-coated 96-well plates (Thermo) and wells were blocked with 1% bovine serum albumin (BSA) (w/v) in 20 mM HEPES, 100 mM NaCl, 5 mM $CaCl_2$, pH 7.4, 0.05% Tween 20 (v/v) (HBSC-T). Seven four-fold serial dilutions of peptide competitors were prepared in solution with 1 μM HA-tagged tEGF-A in HBSC-T before adding to the PCSK9-coated wells for 2 h at 37 °C. tEGF-A, TEX-S3_01, and TEX-S3_02 were tested from 160 μM, TEX-S2_02 was tested from 16 μM, TEX-S2_03 was tested from 40 μM. The wells were washed briefly with HBSC-T then incubated with anti-HA antibody (1:1000 dilution in 0.1% BSA in HBSC-T (w/v), Thermo) in 0.1 % BSA in HBSC-T (w/v) for 45 min at RT. The wells were washed three times with HBSC-T, then incubated with goat anti-mouse IgG-HRP antibody (1:2000 dilution in 0.1% BSA in HBSC-T (w/v), Thermo) for 45 min at RT. The wells were washed a further three times with HBSC-T before addition of TMB substrate solution (Thermo). After 20 min the reaction was quenched with 0.5 M H_2SO_4 before measuring the absorbance using a Tecan Infinite M1000 Pro plate reader. The IC_{50} values were calculated by plotting non-linear regression using the log(inhibitor) vs. response – variable

slope (four parameters) in GraphPad Prism. IC_{50} values were the average ± s.d. of three independent experiments, and 95% confidence intervals were calculated.

ITC binding

All measurements were performed on a MicroCal 200 iTC instrument. PCSK9 was loaded in the sample cell at 20 μM and peptides were loaded into the syringe at 200 μM using a running buffer of 50 mM HEPES pH 7.4, 100 mM NaCl, 5 mM $CaCl_2$. Each titration experiment consisted of an initial 1 μL injection followed by 13 injections of 3.22 μL with a stirring speed of 1,000 rpm at 25 °C. Data were fitted to a one-site binding model, and each peptide was tested in one independent experiment.

Cell culture conditions

The HepG2 cell line was cultured in Dulbecco's modified Eagle's medium (DMEM) high glucose with stable L-glutamine supplemented with 10% fetal bovine serum (FBS), 100 U mL^{-1} penicillin, 100 μg mL^{-1} streptomycin, and incubated at 37 °C under 5% CO_2 atmosphere. HepG2 cells were used for no more than 20 passages after thawing.

LDLR on cell-western

Experiments were performed as previously described.[32] HepG2 cells (3.0×10^4 $well^{-1}$) were seeded in 96-well plates and the following day, cells were starved overnight in DMEM without FBS. Cells were treated with either 4 μg mL^{-1} PCSK9 or 4 μg mL^{-1} PCSK9 with either tEGF-A (0.5–50 μM), TEX-S2_03 (0.05–5 μM), TEX-S3_01 (0.5-50 μM), or vehicle (H_2O) for 2 h at 37 °C under 5% CO_2 atmosphere. Treated HepG2 cells were fixed in 4% paraformaldehyde

for 20 min at RT. Cells were washed with phosphate buffered saline pH 7.4 (PBS) and the endogenous peroxides activity was quenched by adding 3% H_2O_2 in PBS for 20 min at RT. Non-specific sites were blocked with 5% BSA in PBS (w/v) for 1.5 h at RT. LDLR primary antibody solution (1:3000 in 5% BSA in PBS (w/v), Pierce) was incubated overnight at 4 °C. Subsequently, the primary antibody solution was discarded and each sample was washed with PBS. Goat anti-rabbit Ig-HRP secondary antibody solution (1:6000 in 5% BSA in PBS (w/v), Pierce) was added and incubated 1 h at RT. The secondary antibody solution was washed with PBS. TMB substrate solution (Pierce) was added and the plate was incubated at RT until the desired color was developed. The reaction was then stopped with 2 M H_2SO_4 and the absorbance at 450 nm was measured using the Synergy H1 fluorescent plate reader (Biotek). Cells were stained with Janus green stain (Abcam) before 0.5 M HCl was added per well. The OD at 595 nm was measured using the Synergy H1 fluorescent plate reader. Data are presented as mean ± s.d. of three independent experiments, each performed with three replicates, using GraphPad Prism. Statistical analyses were carried out by student t-test. *P*-values < 0.05 were considered to be significant.

LDL uptake assay

Experiments were performed as previously described.[35] HepG2 cells (3.0 x 10^4 $well^{-1}$) were seeded in black 96-well plates and kept in complete growth medium for 2 d before treatment. The third day, they were treated with either 4 µg/mL PCSK9, or 4 µg/mL PCSK9 with either tEGF-A (0.5–50 µM), TEX-S2_03 (0.05–5 µM), or TEX-S3_01 (0.05–50 µM), or vehicle (H_2O) for 2 h with at 37 °C under 5% CO_2 atmosphere. At the end of the treatments, the culture medium was replaced with LDL-DyLight™ 550 working solution (Cayman Chemical Company). The cells were additionally incubated for 2 h at 37 °C and then the culture medium

was aspirated and replaced with PBS. The degree of LDL uptake was measured using the Synergy H1 fluorescent plate reader (excitation and emission wavelengths 540 and 570 nm, respectively). Data were the average ± s.d. of three independent experiments, each performed with three replicates, using GraphPad Prism. Statistical analyses were carried out by student t-test. *P*-values < 0.05 were considered to be significant.

MTT cell toxicity assay

HepG2 cells (3.0 x 10^4 $well^{-1}$) were treated with tEGF-A (0.5–100 μM), TEX-S2_03 (0.05–50 μM), TEX-S3_01 (0.5–100 μM), or vehicle (H_2O) in complete growth media for 48 h at 37 °C under 5% CO_2 atmosphere. Peptide solutions were aspirated and 0.5 mg/mL 3-(4,5-dimethylthiazol-2-yl)-2,5-diphenyltetrazolium bromide (MTT) filtered solution was added for 2 h at 37 °C under 5% CO_2 atmosphere. Lysis buffer was added, and the absorbance was normalized at 570 nm before reading the value at 630 nm on the synergy H1 fluorescence plate reader. Data were the average ± s.d. of three independent experiments, each performed with three replicates, using GraphPad Prism. Statistical analyses were carried out by student t-test. *P*-values < 0.05 were considered to be significant.

SUPPORTING INFORMATION

Supporting Information Available: This material is available free of charge *via* the Internet. MiSeq next generation sequencing data for TEX-S2 and TEX-S3; 1D ^{1}H NMR spectra for TEX-S2_03; ITC binding isotherms; cell viability assays; HPLC chromatograms and ESI-MS spectra of peptides.

Notes

The authors declare no competing interests.

ACKNOWLEDGEMENTS

Work in our laboratory on PCSK9 antagonists is supported by a grant from the National Health and Medical Research Council (APP1107403) and by access to the facilities of the Australian Research Council Centre of Excellence for Innovations in Peptide and Protein Science (CE200100012). DJC is an Australian Research Council (ARC) Australian Laureate (FL150100146). The authors would like to thank E. Gilding for helpful discussions regarding the sequencing of the phage libraries.

References

1. Roth, G. A.; Johnson, C.; Abajobir, A.; Abd-Allah, F.; Abera, S. F.; Abyu, G.; Ahmed, M.; Aksut, B.; Alam, T.; Alam, K., et al. (2017) Global, regional, and national burden of cardiovascular diseases for 10 causes, 1990 to 2015. *J. Am. Coll. Cardiol. 70*, 1-25.

2. Ference, B. A.; Ginsberg, H. N.; Graham, I.; Ray, K. K.; Packard, C. J.; Bruckert, E.; Hegele, R. A.; Krauss, R. M.; Raal, F. J.; Schunkert, H.; Watts, G. F.; Borén, J.; Fazio, S.; Horton, J. D.; Masana, L.; Nicholls, S. J.; Nordestgaard, B. G.; van de Sluis, B.; Taskinen, M.-R.; Tokgözoğlu, L.; Landmesser, U.; Laufs, U.; Wiklund, O.; Stock, J. K.; Chapman, M. J.; Catapano, A. L. (2017) Low-density lipoproteins cause atherosclerotic cardiovascular disease. 1. Evidence from genetic, epidemiologic, and clinical studies. A consensus statement from the European Atherosclerosis Society Consensus Panel. *Eur. Heart J. 38*, 2459-2472.

3. Akyea, R. K.; Kai, J.; Qureshi, N.; Iyen, B.; Weng, S. F. (2019) Sub-optimal cholesterol response to initiation of statins and future risk of cardiovascular disease. *Heart 105*, 975-981.

4. Rallidis, L. S. (2020) The changing landscape of lipid-lowering therapy after the new ESC/EAS guidelines for the management of dyslipidaemias: Launching the era of triple hypolipidaemic therapy in very high risk patients. *Atherosclerosis 292*, 231-233.

5. Benjannet, S.; Rhainds, D.; Essalmani, R.; Mayne, J.; Wickham, L.; Jin, W.; Asselin, M.-C.; Hamelin, J.; Varret, M.; Allard, D.; Trillard, M.; Abifadel, M.; Tebon, A.; Attie, A. D.; Rader, D. J.; Boileau, C.; Brissette, L.; Chrétien, M.; Prat, A.; Seidah, N. G. (2004) NARC-1/PCSK9 and its natural mutants: Zymogen cleavage and effects on the low density lipoprotein (LDL) receptor and LDL cholesterol. *J. Biol. Chem. 279*, 48865-48875.

6. Park, S. W.; Moon, Y.-A.; Horton, J. D. (2004) Post-transcriptional regulation of low density lipoprotein receptor protein by proprotein convertase subtilisin/kexin type 9a in mouse liver. *J. Biol. Chem. 279*, 50630-50638.

7. Maxwell, K. N.; Breslow, J. L. (2004) Adenoviral-mediated expression of Pcsk9 in mice results in a low-density lipoprotein receptor knockout phenotype. *Proc. Natl. Acad. Sci. U. S. A. 101*, 7100-7105.

8. Abifadel, M.; Varret, M.; Rabès, J.-P.; Allard, D.; Ouguerram, K.; Devillers, M.; Cruaud, C.; Benjannet, S.; Wickham, L.; Erlich, D.; Derré, A.; Villéger, L.; Farnier, M.; Beucler, I.; Bruckert, E.; Chambaz, J.; Chanu, B.; Lecerf, J.-M.; Luc, G.; Moulin, P.; Weissenbach, J.; Prat, A.; Krempf, M.; Junien, C.; Seidah, N. G.; Boileau, C. (2003) Mutations in PCSK9 cause autosomal dominant hypercholesterolemia. *Nat. Genet. 34*, 154.

9. Lambert, G.; Sjouke, B.; Choque, B.; Kastelein, J. J. P.; Hovingh, G. K. (2012) The PCSK9 decade. *J. Lipid Res. 53*, 2515-2524.

10. Mullard, A. (2017) Nine paths to PCSK9 inhibition. *Nat. Rev. Drug Discov. 16*, 299-301.

11. Warden, B. A.; Fazio, S.; Shapiro, M. D. (2020) The PCSK9 revolution: Current status, controversies, and future directions. *Trends Cardiovasc. Med. 30*, 179-185.

12. Lagace, T. A.; Curtis, D. E.; Garuti, R.; McNutt, M. C.; Park, S. W.; Prather, H. B.; Anderson, N. N.; Ho, Y. K.; Hammer, R. E.; Horton, J. D. (2006) Secreted PCSK9 decreases the number of LDL receptors in hepatocytes and inlivers of parabiotic mice. *J. Clin. Invest. 116*, 2995-3005.

13. Zhang, D.-W.; Lagace, T. A.; Garuti, R.; Zhao, Z.; McDonald, M.; Horton, J. D.; Cohen, J. C.; Hobbs, H. H. (2007) Binding of proprotein convertase subtilisin/kexin type 9 to epidermal growth factor-like repeat A of low density lipoprotein receptor decreases receptor recycling and increases degradation. *J. Biol. Chem. 282*, 18602-18612.

14. Gu, H.-M.; Adijiang, A.; Mah, M.; Zhang, D.-W. (2013) Characterization of the role of EGF-A of low density lipoprotein receptor in PCSK9 binding. *J. Lipid Res. 54*, 3345-3357.

15. Kwon, H. J.; Lagace, T. A.; McNutt, M. C.; Horton, J. D.; Deisenhofer, J. (2008) Molecular basis for LDL receptor recognition by PCSK9. *Proc. Natl. Acad. Sci. U. S. A. 105*, 1820-1825.

16. Bottomley, M. J.; Cirillo, A.; Orsatti, L.; Ruggeri, L.; Fisher, T. S.; Santoro, J. C.; Cummings, R. T.; Cubbon, R. M.; Lo Surdo, P.; Calzetta, A.; Noto, A.; Baysarowich, J.; Mattu, M.; Talamo, F.; De Francesco, R.; Sparrow, C. P.; Sitlani, A.; Carfí, A. (2009) Structural and biochemical characterization of the wild type PCSK9-EGF(AB) complex and natural familial hypercholesterolemia mutants. *J. Biol. Chem. 284*, 1313-1323.

17. Lo Surdo, P.; Bottomley, M. J.; Calzetta, A.; Settembre, E. C.; Cirillo, A.; Pandit, S.; Ni, Y. G.; Hubbard, B.; Sitlani, A.; Carfí, A. (2011) Mechanistic implications for LDL receptor degradation from the PCSK9/LDLR structure at neutral pH. *EMBO Rep. 12*, 1300-1305.

18. Chan, J. C. Y.; Piper, D. E.; Cao, Q.; Liu, D.; King, C.; Wang, W.; Tang, J.; Liu, Q.; Higbee, J.; Xia, Z., et al. (2009) A proprotein convertase subtilisin/kexin type 9 neutralizing antibody reduces serum cholesterol in mice and nonhuman primates. *Proc. Natl. Acad. Sci. U. S. A. 106*, 9820-9825.

19. Sabatine, M. S.; Giugliano, R. P.; Keech, A. C.; Honarpour, N.; Wiviott, S. D.; Murphy, S. A.; Kuder, J. F.; Wang, H.; Liu, T.; Wasserman, S. M.; Sever, P. S.; Pedersen, T. R. (2017) Evolocumab and clinical outcomes in patients with cardiovascular disease. *N. Engl. J. Med. 376*, 1713-1722.

20. Schwartz, G. G.; Steg, P. G.; Szarek, M.; Bhatt, D. L.; Bittner, V. A.; Diaz, R.; Edelberg, J. M.; Goodman, S. G.; Hanotin, C.; Harrington, R. A.; Jukema, J. W.; Lecorps, G.; Mahaffey, K. W.; Moryusef, A.; Pordy, R.; Quintero, K.; Roe, M. T.; Sasiela, W. J.; Tamby, J.-F.; Tricoci, P.; White, H. D.; Zeiher, A. M. (2018) Alirocumab and cardiovascular outcomes after acute coronary syndrome. *N. Engl. J. Med. 379*, 2097-2107.

21. Wong, N. D.; Shapiro, M. D. (2019) Interpreting the findings from the recent PCSK9 monoclonal antibody cardiovascular outcomes trials. *Front. Cardiovasc. Med. 6*, 1-7.

22. Azari, S.; Rezapour, A.; Omidi, N.; Alipour, V.; Behzadifar, M.; Safari, H.; Tajdini, M.; Bragazzi, N. L. (2019) Cost-effectiveness analysis of PCSK9 inhibitors in cardiovascular diseases: a systematic review. *Heart Fail. Rev. 25*, 1077-1088.

23. Scherer, D. J.; Nelson, A. J.; O'Brien, R.; Kostner, K. M.; Hare, D. L.; Colquhoun, D. M.; Barter, P. J.; Aylward, P.; Nicholls, S. J.; Watts, G. F. (2019) Status of PCSK9 monoclonal antibodies in Australia. *Heart Lung Circ. 28*, 1571-1579.

24. Nishikido, T.; Ray, K. K. (2019) Non-antibody approaches to proprotein convertase subtilisin kexin 9 inhibition: siRNA, antisense oligonucleotides, adnectins, vaccination, and new attempts at small-molecule inhibitors based on new discoveries. *Front. Cardiovasc. Med. 5*, 1-17.

25. Seidah, N. G.; Prat, A.; Pirillo, A.; Catapano, A. L.; Norata, G. D. (2019) Novel strategies to target proprotein convertase subtilisin kexin 9: Beyond monoclonal antibodies. *Cardiovasc. Res. 115*, 510-518.

26. Craik, D. J.; Fairlie, D. P.; Liras, S.; Price, D. (2013) The future of peptide-based drugs. *Chem. Biol. Drug Des. 81*, 136-147.

27. Lau, J. L.; Dunn, M. K. (2018) Therapeutic peptides: Historical perspectives, current development trends, and future directions. *Bioorg. Med. Chem. 26*, 2700-2707.

28. Nevola, L.; Giralt, E. (2015) Modulating protein–protein interactions: The potential of peptides. *Chem. Commun. 51*, 3302-3315.

29. Zhang, Y.; Eigenbrot, C.; Zhou, L.; Shia, S.; Li, W.; Quan, C.; Tom, J.; Moran, P.; Di Lello, P.; Skelton, N. J.; Kong-Beltran, M.; Peterson, A.; Kirchhofer, D. (2014) Identification of a small peptide that inhibits PCSK9 protein binding to the low density lipoprotein receptor. *J. Biol. Chem. 289*, 942-955.

30. Zhang, Y.; Ultsch, M.; Skelton, N. J.; Burdick, D. J.; Beresini, M. H.; Li, W.; Kong-Beltran, M.; Peterson, A.; Quinn, J.; Chiu, C.; Wu, Y.; Shia, S.; Moran, P.; Di Lello, P.; Eigenbrot, C.; Kirchhofer, D. (2017) Discovery of a cryptic peptide-binding site on PCSK9 and design of antagonists. *Nat. Struct. Mol. Biol. 24*, 848-856.

31. Burdick, D. J.; Skelton, N. J.; Ultsch, M.; Beresini, M. H.; Eigenbrot, C.; Li, W.; Zhang, Y.; Nguyen, H.; Kong-Beltran, M.; Quinn, J. G.; Kirchhofer, D. (2020) Design of organo-peptides as bipartite PCSK9 antagonists. *ACS Chem. Biol. 15*, 425-436.

32. Tombling, B. J.; Lammi, C.; Lawrence, N.; Gilding, E. K.; Grazioso, G.; Craik, D. J.; Wang, C. K. (2020) Bioactive cyclization optimizes the affinity of a proprotein convertase subtilisin/kexin type 9 (PCSK9) peptide inhibitor. *J. Med. Chem.*, DOI:10.1021/acs.jmedchem.0c01766.

33. Stucchi, M.; Grazioso, G.; Lammi, C.; Manara, S.; Zanoni, C.; Arnoldi, A.; Lesma, G.; Silvani, A. (2016) Disrupting the PCSK9/LDLR protein–protein interaction by an imidazole-based minimalist peptidomimetic. *Org. Biomol. Chem. 14*, 9736-9740.

34. Lammi, C.; Sgrignani, J.; Arnoldi, A.; Lesma, G.; Spatti, C.; Silvani, A.; Grazioso, G. (2019) Computationally driven structure optimization, synthesis, and biological evaluation of imidazole-based proprotein convertase subtilisin/kexin 9 (PCSK9) inhibitors. *J. Med. Chem. 62*, 6163-6174.

35. Lammi, C.; Zanoni, C.; Aiello, G.; Arnoldi, A.; Grazioso, G. (2016) Lupin peptides modulate the protein-protein interaction of PCSK9 with the low density lipoprotein receptor in HepG2 cells. *Sci. Rep. 6*, 29931.

36. Grazioso, G.; Bollati, C.; Sgrignani, J.; Arnoldi, A.; Lammi, C. (2018) First food-derived peptide inhibitor of the protein–protein interaction between gain-of-function PCSK9D374Y and the low-density lipoprotein receptor. *J. Agric. Food Chem. 66*, 10552-10557.

37. Lammi, C.; Sgrignani, J.; Roda, G.; Arnoldi, A.; Grazioso, G. (2019) Inhibition of PCSK9D374Y/LDLR protein–protein interaction by computationally designed T9 lupin peptide. *ACS Med. Chem. Lett. 10*, 425-430.

38. Fuentes-Prior, P.; Iwanaga, Y.; Huber, R.; Pagila, R.; Rumennik, G.; Seto, M.; Morser, J.; Light, D. R.; Bode, W. (2000) Structural basis for the anticoagulant activity of the thrombin–thrombomodulin complex. *Nature 404*, 518-525.

39. Luca, V. C.; Jude, K. M.; Pierce, N. W.; Nachury, M. V.; Fischer, S.; Garcia, K. C. (2015) Structural basis for Notch1 engagement of Delta-like 4. *Science 347*, 847-853.

40. Vinther, T. N.; Norrman, M.; Ribel, U.; Huus, K.; Schlein, M.; Steensgaard, D. B.; Pedersen, T. Å.; Pettersson, I.; Ludvigsen, S.; Kjeldsen, T.; Jensen, K. J.; Hubálek, F. (2013) Insulin analog with additional disulfide bond has increased stability and preserved activity. *Protein Sci. 22*, 296-305.

41. Wang, C. K.; Swedberg, J. E.; Northfield, S. E.; Craik, D. J. (2015) Effects of cyclization on peptide backbone dynamics. *J. Phys. Chem. B 119*, 15821-15830.

42. Góngora-Benítez, M.; Tulla-Puche, J.; Albericio, F. (2014) Multifaceted roles of disulfide bonds. Peptides as therapeutics. *Chem. Rev. 114*, 901-926.

43. Tombling, B. J.; Wang, C. K.; Craik, D. J. (2020) EGF-like and other disulfide-rich microdomains as therapeutic scaffolds. *Angew. Chem. Int. Ed. 59*, 11218-11232.

44. Wang, C. K.; Craik, D. J. (2018) Designing macrocyclic disulfide-rich peptides for biotechnological applications. *Nat. Chem. Biol. 14*, 417-427.

45. Shan, L.; Pang, L.; Zhang, R.; Murgolo, N. J.; Lan, H.; Hedrick, J. A. (2008) PCSK9 binds to multiple receptors and can be functionally inhibited by an EGF-A peptide. *Biochem. Biophys. Res. Commun. 375*, 69-73.

46. Zhang, Y.; Zhou, L.; Kong-Beltran, M.; Li, W.; Moran, P.; Wang, J.; Quan, C.; Tom, J.; Kolumam, G.; Elliott, J. M.; Skelton, N. J.; Peterson, A. S.; Kirchhofer, D. (2012) Calcium-

1 independent inhibition of PCSK9 by affinity-improved variants of the LDL receptor EGF(A)
2 domain. *J. Mol. Biol. 422*, 685-696.
3 47. Schroeder, C. I.; Swedberg, J. E.; Withka, J. M.; Rosengren, K. J.; Akcan, M.; Clayton,
4 D. J.; Daly, N. L.; Cheneval, O.; Borzilleri, K. A.; Griffor, M.; Stock, I.; Colless, B.; Walsh,
5 P.; Sunderland, P.; Reyes, A.; Dullea, R.; Ammirati, M.; Liu, S.; McClure, K. F.; Tu, M.;
6 Bhattacharya, S. K.; Liras, S.; Price, D. A.; Craik, D. J. (2014) Design and synthesis of
7 truncated EGF-A peptides that restore LDL-R recycling in the presence of PCSK9 in vitro.
8 *Chem. Biol. 21*, 284-294.
9 48. Wang, C. K.; Ghani, H. A.; Bundock, A.; Weidmann, J.; Harvey, P. J.; Edwards, I. A.;
10 Schroeder, C. I.; Swedberg, J. E.; Craik, D. J. (2018) Calcium-mediated allostery of the EGF
11 fold. *ACS Chem. Biol. 13*, 1659-1667.
12 49. Claveria-Gimeno, R.; Vega, S.; Abian, O.; Velazquez-Campoy, A. (2017) A look at
13 ligand binding thermodynamics in drug discovery. *Expert Opin. Drug Discov. 12*, 363-377.
14 50. Kirchhofer, D.; Burdick, D. J.; Skelton, N. J.; Zhang, Y.; Ultsch, M. (2020) Regions of
15 conformational flexibility in the proprotein convertase PCSK9 and design of antagonists for
16 LDL cholesterol lowering. *Biochem. Soc. Trans. 48*, 1323-1336.
17 51. Ikezoe, T.; Yang, J.; Nishioka, C.; Pan, B.; Xu, K.; Furihata, M.; Nakamura, K.;
18 Yurimoto, H.; Sakai, Y.; Honda, G.; Yokoyama, A. (2017) The fifth epidermal growth factor-
19 like region of thrombomodulin exerts cytoprotective function and prevents SOS in a murine
20 model. *Bone Marrow Transplant. 52*, 73-79.
21 52. Pan, B.; Wang, X.; Kojima, S.; Nishioka, C.; Yokoyama, A.; Honda, G.; Xu, K.; Ikezoe,
22 T. (2017) The fifth EGF-like region of thrombomodulin alleviates murine graft-versus-host
23 disease in a G-protein coupled receptor 15 dependent manner. *Biol. Blood Marrow Transplant.*
24 *23*, 746-756.

53. Crooks, G. E.; Hon, G.; Chandonia, J.-M.; Brenner, S. E. (2004) WebLogo: A sequence logo generator. *Genome Res. 14*, 1188-1190.

54. Webb, B.; Sali, A. (2016) Comparative protein structure modeling using MODELLER. *Curr. Protoc. Bioinformatics 54*, 5.6.1-5.6.37.

55. Harvey, M. J.; Giupponi, G.; Fabritiis, G. D. (2009) ACEMD: Accelerating biomolecular dynamics in the microsecond time scale. *J. Chem. Theory Comput. 5*, 1632-1639.

56. Humphrey, W.; Dalke, A.; Schulten, K. (1996) VMD: Visual molecular dynamics. *J. Mol. Graph. 14*, 33-38.

1 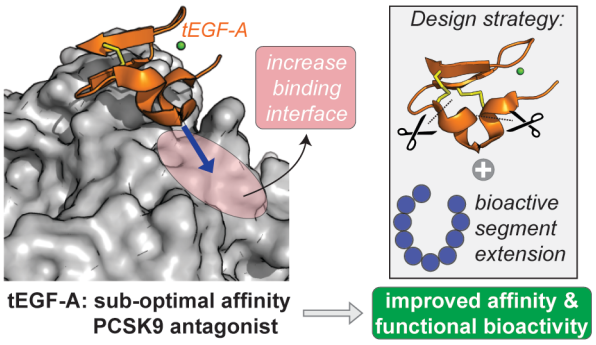

2 **TOC graphic**